Markov random field-based segmentation algorithm for the images of cotton plants taken from unmanned aerial vehicles

Qianqian Zhen and Huichao Gu

School of Software Engineering, Anyang Normal University, Anyang 455000, Henan, China

Received: 16.06.2022

Abstract. Segmentation of aerial images of crop is an important method for the crop prediction and analysis based on plant-protecting unmanned aerial vehicles (UAVs). The problem is that the accuracy of traditional crop-image segmentation based on a super-green feature is not high enough and, moreover, the corresponding algorithm can reveal great differences in the precision for different crops. In this study, we use a Markov random-field segmentation model for the aerial images taken from the plant-protecting UAVs. A standard K-mean algorithm is employed to mark the observation field and the model parameters are estimated by an expectation-maximization method. For deriving the segmentation results, an iterated conditional-modes algorithm is applied. The experimental results testify that the approach of Markov random fields can segment efficiently the cotton-plant images obtained from the UAVs. Then the segmentation accuracy becomes higher and the algorithm adaptability better. However, the processing time increases and the real-time regime can be questioned when the number of segmented image pixels exceeds a critical value.

Keywords: image segmentation, Markov random fields, iterated conditional-modes algorithm, unmanned aerial vehicles for plant protection

UDC: 004.932.2

1. Introduction

Rapid and accurate monitoring and evaluation of crop growth is one of the key issues in precision agriculture. It is also a basis for collecting important agricultural information and machinery automation, which has become a hotspot in the field of agricultural production in the recent years. At present, applications of computer-vision technologies in agriculture have become more and more frequent. They include monitoring and evaluating of crop information, yield prediction, weeding, pest control, etc. Image segmentation is the most important technical part of the appropriate problems [1].

Unmanned aerial vehicles (UAVs) aimed at protecting plants have many advantages such as high efficiency, small amount of liquids sprayed per unit area, no need in special airports for taking off and landing, and good maneuverability. Moreover, the UAVs for the plant protection can be operated remotely, thus avoiding fundamentally a risk for operators to be exposed to pesticides and improving the working conditions of those operators. Driven by a precision agriculture and a large-scale planting, the plant-protecting UAVs have demonstrated their outstanding advantages in such areas as operation of paddy fields and high-stalk crop fields, a quick response to pests and diseases, etc. [2]. Under real-life operating conditions, the relevant natural environment is complex and changeable and, moreover, there are notable differences in the shapes of different crops. The abilities of autonomous navigation and path-planning for the plant-protection UAVs are limited by the crop-image extraction. As a consequence, the image-segmentation algorithms used for the plant-protecting UAVs are of primary importance.

Although the common methods of green-crop detection are based on so-called super-green features and morphological processing, the corresponding segmentation accuracy is not sufficiently high. Besides, the accuracies of the same algorithm applied to segmentation of different crops can be enormously different.

Recently, many scholars have adopted a method of Markov random fields (MRF) for image segmentation. The MRF has been widely used in many brunches of science and technology. In Ref. [3], the MRF and a mixed kernel-function clustering have been applied to the problem of brain-tumour image segmentation. Gaussian prior and Markov random-field constraints have been applied in a pre-stack seismic inversion by Xiaoshuang et al. [4]. The MRF has also been applied to the analysis of development of karsts [5]. L. Ning et al. [6] have suggested an improved MRF version to segment defect-involving images associated with stamping. Zhang Ling et al. [7] have offered the MRF to identify damaged buildings in the single-phase seismic images, while Li Pengju et al. have used the improved MRF in event-camera denoising [8].

Besides of the MRF, deep machine learning is also acquiring some popularity in image segmentation. As a single example, A. Feng et al. have used this approach to evaluate the germination of cotton plants [9]. Note that the deep-learning algorithms manifest high enough segmentation speed and accuracy, although they require a large amount of data. One has to note in this respect that the datasets of cotton seedlings are relatively scarce and so the annotation tasks are difficult. Since we are mainly interested in the segmentation of test cotton fields, which is characterized by a small amount of data, the deep-learning approach can be not better than the traditional segmentation methods.

The subject of the present study is aerial photographs of cotton seedlings. Below we will demonstrate that the segmentation accuracy can be greatly improved and the real-time performance can be provided by an improved Markov-based iterated conditional-modes (ICM) algorithm. In particular, the algorithm suggested by us has a higher accuracy than that of the traditional crop-extraction methods based on the super-green features, while the navigation and operation of the plant-protecting UAVs become more intelligent (see Ref. [2]).

2. Markov random field

The MRF is often used in the field of computer vision to model different pixel-level image features. Due to equivalence of the MRF and Gibbs distributions, the joint distribution of the MRF can be transformed to a simple form. The cost function can be derived by a Bayesian-based maximum a posteriori (MAP) estimation, so that the problem of image segmentation can be transformed into the problem of cost-function optimization [10, 11].

A canonical Markov process describes a sequence of random states in time. Suppose that a random process generates a random state Z at time t. Then the random state appearing after the time moment t is linked only with the state Z and has nothing to do with the random states occurring before this moment. This memoryless process is called a Markov process [12, 13]. By analogy, the Markov process in the image processing describes a relationship between the state and the spatial coordinates of pixels. The state (or the category) of a given pixel is related only to the category of the pixels in its neighbourhood and does not depend on the characteristics of more distant pixels. Suppose that every point in the space $S = \left\{ s = (i, j) \middle| 1 \le i \le M, 1 \le j \le N \right\}$ corresponds to a random variable $X = \left\{ X_s \middle| s \in S \right\}$. Then $X = \left\{ X_s \middle| s \in S \right\}$ is called a random field on S (see Fig. 1).

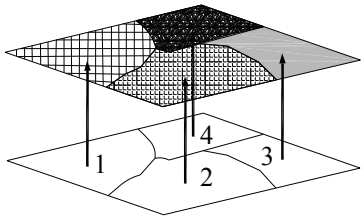

Fig. 1. Illustration of *S*-field and *X*-field in a Markov random field (see the text and Ref. [14] for more details).

Here $X_s = x_s$ is given by $\left(X_1 = x_1, ..., X_{MN} = x_{MN}\right)$, which can be simplified to $X = x$ (with *M* being the number of pixels that fit into the image width and *N* the number of pixels along the image height). Let $x = \left\{x_1, x_2, ..., x_{MN}\right\}$ constitute a set of all possible random states Ω_X on *S*. When Ω_X is a random marking field, the probability $P\left(X_s = x_s\right)$ for any random variable $X_s = x_s$ can be written as $P\left(x_s\right)$, whereas the joint probability $P\left(X = x\right)$ can be simplified to $P\left(x\right)$.

The random field X exists in the probability space $\left(\Omega, S, P\right)$ if and only if we have the inequality $P\left(x\right) > 0$, where

$$P\left(x_s \left| x_{S\setminus\{s\}}\right.\right) = P\left(x_s \left| x_{N_s}\right.\right). \tag{1}$$

Having defined the random field X on the probability space $\left(\Omega, S, P\right)$, we obtain the MRF with respect to the neighbourhood system $N = \left\{N_s \left| \forall s \in S\right.\right\}$. Here $S \setminus \{ s \}$ denotes the point set that excludes s in the grid S, and N_s denotes the neighbourhood of the node s referring to the set of all the points adjacent to this node.

3. MRF-MAP segmentation model

A maximum-likelihood estimation (MLE) provides the idea of solving a Markov marker-field model for a given observation field. When the regularized solution process introduces a priori parameters, the MLE becomes the maximum posterior-probability estimation, MAP. The difference between the MAP and the MLE in the pixel space is that the MLE believes that the probability of each pixel being marked as a certain class is uniform, while the MAP incorporates the label probability distribution brought by the model parameters themselves.

The characteristic $S = \left\{s_1, s_2, ..., s_{MN}\right\}$ involves all the image pixels belonging to the set $M \times N$. The observation field $Y = \left\{y_S \left| s \in S\right.\right\}$ corresponds to the aerial-image data, while each element represented by the marker field selects a category tag from the category space. The marker field $X = \left\{x_s \left| s \in S\right.\right\}$ indicates that each element of S selects a category tag in the category space $L = \left\{1, 2, ..., l\right\}$.

When the observation field is specified, the Bayesian posterior-probability criterion is given by

$$P\left(X = x \left| Y = y\right.\right) = \frac{P\left(Y = y \left| X = x\right.\right) P\left(X = x\right)}{P\left(Y = y\right)}, \tag{2}$$

which can be simplified to

$$P\left(X \left| Y\right.\right) \propto P\left(Y \left| X\right.\right) P\left(X = x\right). \tag{3}$$

In its turn, the expression for the energy is as follows:

$$X^* \propto \arg\max P(Y|X)P(X=x) \propto \arg\min U(X,Y) = \arg\min\left[U_1(X)+U_2(Y|X)\right], \quad (4)$$

where $U(X,Y)$ is the overall system-energy function, $U_1(X)$ the energy function of the marker-field prior model, and $U_2(Y|X)$ the energy function of the observation field under the conditional probability. One can obtain from the above formula that the image segmentation represents a process of minimizing the posterior energy function [15]. The modelling steps of the MRF-MAP segmentation model are illustrated in Fig. 2.

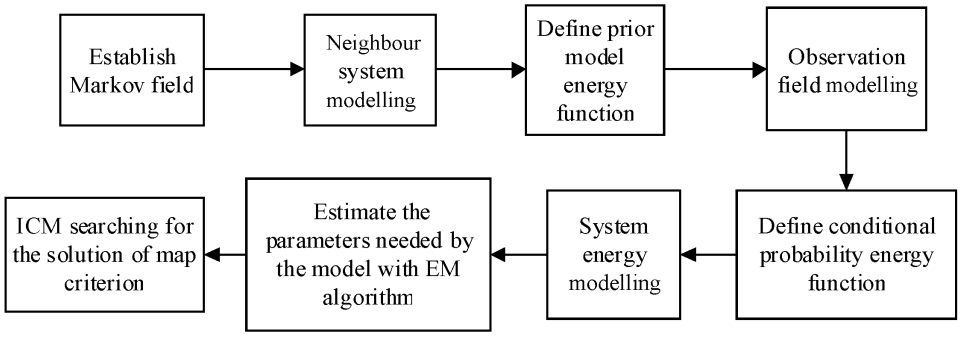

Fig. 2. Schematic explanation of an MRF-MAP segmentation model: 'EM' denotes 'expectation–maximization'.

3.1. System energy function

3.1.1. Prior model energy function. A Hammersley–Clifford theorem gives the equivalence relationship for the MRF and Gibbs random field, i.e. the prior probability of the MRF follows the Gibbs distribution [16]. The neighbourhood system adopts a homogeneous and isotropic second-order 8-neighbourhood. The corresponding mathematical model is given by $N_s^{(2)} = \{(i+1,j+1),(i+1,j),(i+1,j-1),(i,j+1),\ (i,j-1),\ (i-1,j+1),(i-1,j),(i-1,j-1)\}$.

The potential group of the second-order neighbourhood system is shown in Fig. 3. The basic potential group is a binary two-point potential group, while the remaining potential energy is given by $V_{c\neq 2}=0$. Here $U_1(X)$ can be expressed as

$$U_1(X) = \sum_{s\in S} U_1(x_s) = \sum_{s\in S}\sum_{t\in N_s} V_2(x_s,x_t), \quad (5)$$

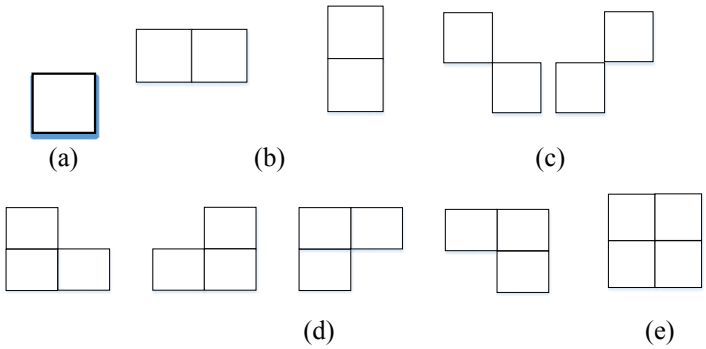

Fig. 3. Potential group of a second-order neighbourhood system: (a) single-point group, (b) horizontal and vertical double-point group, (c) diagonal double-point group, d) triple-point group, and (e) quadruple-point group.

where $V_2(x_s, x_t)$ is a potential function defined by the relation

$$V_2(x_s, x_t) = \begin{cases} -\beta & x_s = x_t \\ +\beta & x_s \neq x_t \end{cases}. \tag{6}$$

Here s denotes the operational pixel, t the second-order 8-neighbourhood pixel of s, x_s and x_t are pixel markers, and β is the penalty factor.

3.1.2. Conditional-probability energy function. The conditional probability $P(Y|X)$ of $U_2(Y|X)$ cannot be obtained directly. Given the marker field X, the sampling pixels in the observation field Y are independent of each other. At the same time, the mathematical model for all pixels in a certain spatial area of a colour image is the Gaussian distribution, so that we have

$$U_2(Y|X) = \sum_{s \in S} \left[(y_s - \mu_k) \Sigma_k^{-1} (y_s - \mu_k)^T + \log|\Sigma_k| \right]. \tag{7}$$

Here $k \in L = \{1, 2, ..., l\}$, μ_k and Σ_k are respectively the mean and the covariance matrix of the class-k Gaussian field, and $k \in L = \{1, 2, ..., l\}$.

The total energy function of the system can be obtained from Eqs. (5) and (7):

$$U(X, Y) = \sum_{s \in S} \sum_{t \in N_s} V_2(x_s, x_t) + \sum_{s \in S} \left[(y_s - \mu_k) \Sigma_k^{-1} (y_s - \mu_k)^T + \log|\Sigma_k| \right]. \tag{8}$$

3.2. Estimates of model parameters with expectation–maximization algorithm.

Let the MLE algorithm be used. In order to derive the parameters $\theta = \{\mu_k, \sigma_k\}$ of the Gaussian distribution, it is necessary to find the θ value at which $\log P(x, y|\theta)$ reaches its maximum. Therefore the calculations are rather complex [17]. In image segmentation we have $z = (x, y)$, where the observation field $\underline{y}$ represents the known data and the label field x corresponds to the hidden unknown category labels of all the pixels. Then an expectation–maximization algorithm can be used to estimate the model parameters. The iterative processes of the expectation–maximization algorithm can be described as follow.

(i) E-step:

$$\beta_s^t = \frac{\pi_k^t P\left(y_s \middle| \mu_k^t, \Sigma_k^t\right)}{\sum_{k=1}^{L} \pi_k^t P\left(y_s \middle| \mu_k^t, \Sigma_k^t\right)}, \tag{9}$$

where β_s^t is the prior probability of the pixel, and π_k^t, μ_k^t and Σ_k^t are the iterative parameters of t.

(ii) M-step:

$$\pi_k^{t+1} = \frac{1}{N} \sum_{s \in S} \beta_s^t, \mu_k^{t+1} = \frac{1}{N \pi_k^t} \sum_{s \in S} \beta_s^t y_s, \Sigma^{t+1} = \frac{1}{N \pi_k^t} \sum_{s \in S} \beta_s^t \left(y_s - \mu_k^{t+1}\right)\left(y_s - \mu_k^{t+1}\right)^T. \tag{10}$$

While iterating continuously the E-steps and M-steps and assigning periodically new values to the π_k^t, μ_k^t and Σ_k^t parameters, one can arrive at stable model parameters.

3.3. ICM algorithm

The ICM is a 'greedy algorithm'. Every time it ignores a global optimal solution and seeks optimal solutions in a certain region instead. Let us operate with each pixel in the space. If the current tag makes the system energy decrease, then one has to update the tag field, otherwise the tag field remains the same. The times needed for updating the marker field are short and so the operation speed is high [18].

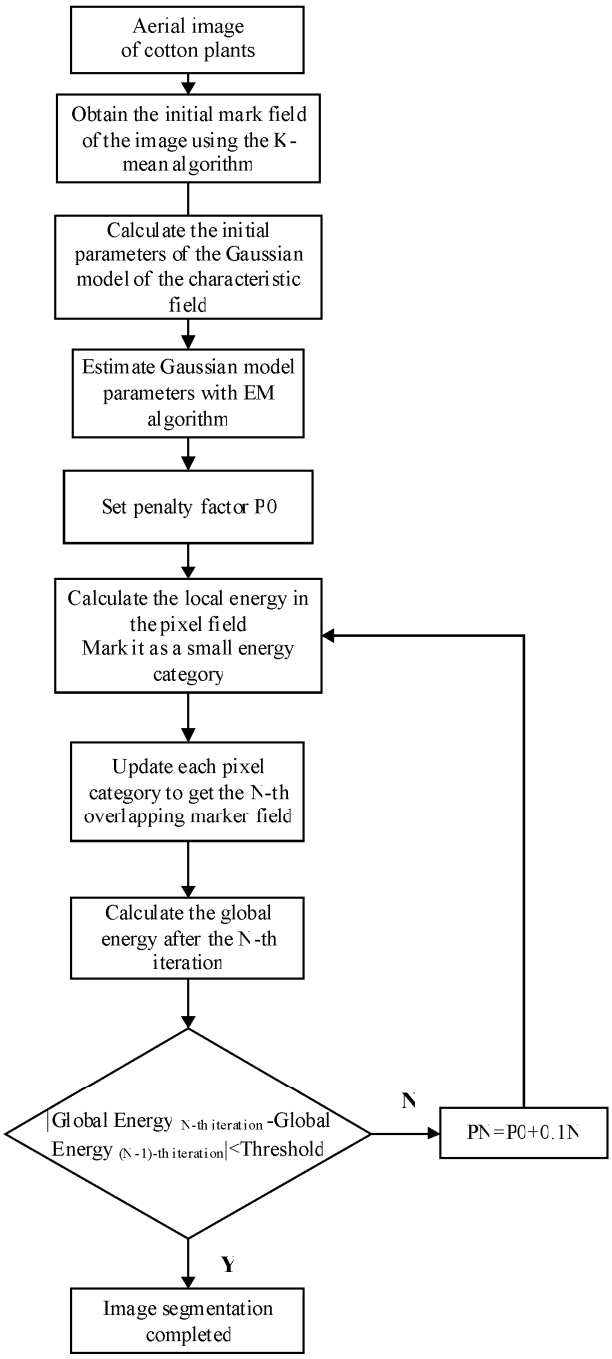

Fig. 4. A flow chart of a Markov-ICM algorithm.

The flow chart of the ICM algorithm is illustrated in Fig. 4 and an image segmented after three initial iterations is shown in Fig. 5. The experiments testify that the results obtained with the three iterations can be segmented to get the main area whenever the background of a cotton-plant image is relatively simple. Although further iterations are more accurate in the boundary-point classification and some pseudo-classified areas can be corrected, the real-time performance is more difficult to achieve for the corresponding procedure. In order to improve the segmentation accuracy and ensure the real-time performance at the same time, it is useful to set a reasonable global-energy threshold. After the initial iteration, morphological filtering can be used to remove a small-area noise.

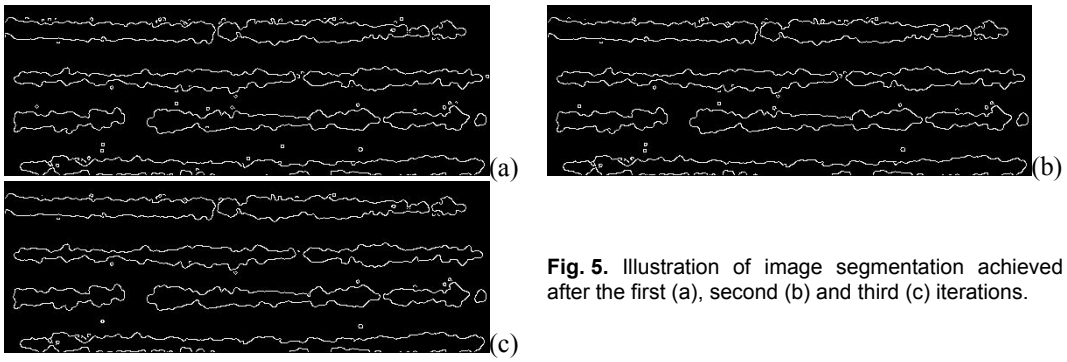

Fig. 5. Illustration of image segmentation achieved after the first (a), second (b) and third (c) iterations.

4. Experimental results and their analysis

In order to test the segmentation results achieved for the aerial images of cotton seedlings taken with different resolutions, we have selected RGB images with the area 1550×551 px^2. The working process of the Markov-ICM-algorithm segmentation is sketched in Fig. 6. For a comparison, the image segmented using the super-green features and the morphological filtering is shown in Fig. 7. There are 250238 target pixels containing cotton seedlings and 155780 target pixels marked by the super-green-features algorithm. On the other hand, the Markov-ICM algorithm finds 232061 target pixels, i.e. it improves the segmentation efficiency by 30.4%. Therefore, a comparison of the segmentation results presented in Fig. 6 and Fig. 7 confirms that the algorithm based upon the super-green features yields in under-segmentation.

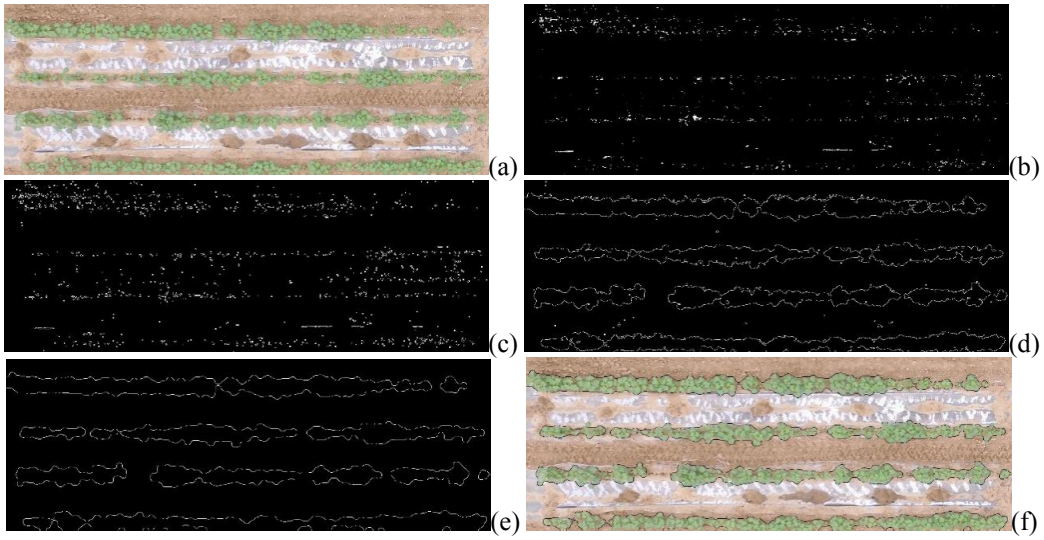

Fig. 6. Experimental implementation of segmentation with the Markov-ICM algorithm: (a) aerial photo of cotton plants, (b) K-mean marker field, (c) initial segmentation and edge extraction, (d) Markov-ICM edge extraction, (e) edge extraction performed after Markov-ICM morphological filtering, and (f) segmentation based on the MRF.

We remind that the segmentation principle associated with the MRF model is based on the energy connection between the image pixels and the field, which provides a high accuracy of segmentation. Moreover, the noises associated with a film and agricultural ruts in the background areas do not interfere with the texture information of the image, thus ensuring an excellent segmentation effect.

Fig. 7. Image segmentation based on super-green features and morphological filtering.

To verify the real-time performance of the Markov-ICM algorithm, we have segmented the images with different pixel sizes and determined the times needed to segment each of these images. The appropriate data are gathered in Table 1. At least above the image area 30000 px^2, the dependence of segmentation time on the image area is perfectly linear, with the Pearson's correlation coefficient larger than 0.999. This linear-in-time property would imply the real-time performance of the underlying algorithm.

Table 1. Segmentation times achieved with the Markov-ICM algorithm for the images with different pixel numbers.

Image width, px	Image height, px	Pixel area, px^2	Segmentation time, s
100	50	5000	1.3267
300	50	15000	1.5661
600	50	30000	1.9030
900	50	45000	3.0189
900	150	135000	6.7619
900	300	270000	11.6119
1200	500	600000	23.5039
1500	500	750000	29.3514
2000	800	1600000	61.9957

5. Conclusion

In this study, the MRF-based segmentation model is used for processing the aerial photos of cotton plants taken by the UAVs. The model parameters are estimated with the expectation–maximization method, while the segmentation results are derived using the ICM optimization algorithm. Our experiments demonstrate that the MRF approach can make a complete account of spatial correlation among the pixels to express properly the prior information involved in the image. This method can efficiently segment the cotton-seedling images obtained by the UAVs. Its only drawback is that, in the process of segmentation, the number of ICM iterations increases with increasing image pixel number. Then the segmentation times become long and the real-time performance needs to be improved.

References

1. Jiang Nan, Dai Jianguo, Xue Jinli, Zhang Guoshun and He Xiangliang, 2021. Cotton growth parameter monitoring based on visible image of UAV and convolutional neural network. J. Shihezi Univ. (Nat. Sci.). **39**: 282–288.

2. Zhou Liwa and Liu Xuelei, 2021. Analysis of the market status and development prospects of the agricultural plant protection UAV industry. Heilongjiang Grain. **11**: 121–122.
3. Wang Zhigang and Feng Yunchao, 2021. Brain tumor image segmentation method based on MRF and mixed kernel function clustering. Electron. Meas. Technol. **44**: 93–97.
4. Xiao Shuang, Ba Jing, Guo Qiang, Fu Li-yun, Guo Qiang, Zhang Lin and Luo Cong, 2020. Research and application of nonlinear pre-stack seismic inversion based on Gaussian prior and Markov random field constraints. Prog. Geophys. **35**: 2250–2258.
5. He GaoFeng, Luo Xianqi, Fan Xunyi and Zhang Yong, 2019. Analysis on karst development laws of tunnels based on the Markov random field. Mod. Tunn. Technol. **56**: 56–64.
6. Lyu Ning, Xiao Jian, Gao, Ouyang Xuefeng and Luo Zhongjie, 2022. Image segmentation algorithm on contour defects for stamping part based on improved MRF. Forg. Stamp. Technol. **47**: 101–109.
7. Zhang Ling, Tan Xuan, Song Dongmei, Wang Bin and Li Rui-lin, 2019. Study on the MRF-based method for damaged buildings extraction from the single-phase seismic image. Seismol. and Geolog. **41**: 1273–1288.
8. Li Pengju, Zhang Yasheng, Fang Yuqiang and Yin Zhiyong, 2021. Denoising algorithm based on improved Markov random field for event camera. Infrared and Laser Engin. **50**: 20210294.
9. Feng A, Zhou J, Vories E and Sudduth K A, 2020. Evaluation of cotton emergence using UAV-based imagery and deep learning. Comp. Electron. Agricult. **177**: 105711.
10. Huang Peng, Zheng Qi and Liang Chao, 2020. Overview of image segmentation methods. Geomat. Inform. Sci. Wuhan Univ. **66**: 519–531.
11. Zheng Xiaonan, Yang Fan and Li Fuzhong, 2020. Overview of crop image segmentation algorithm. Mod. Comp. **19**: 72–75.
12. Wang Chang, Zhang Yongsheng and Wang Xu, 2021. SAR image change detection based on variational method and Markov random field fuzzy local information C-means clustering method. Geom. Inform. Sci. Wuhan Univ. **46**: 844–851.
13. Yan Tinglong, Li Ying and Wang Fengqian, 2022. Recognition and division of aircraft flight action based on MRF model. Comp. Engin. Sci. **44**: 159–164.
14. Zhang Yinhui, 2010. Research on multiscale Markov random fields for image segmentation [PhD Thesis]. Kunming: Kunming University of Science and Technology, China.
15. Zhao Quan-hua, Shi Xue, Wang Yu and Li Yu, 2017. Remote sensing image segmentation of variable class space constrained Gaussian mixture model. J. Commun. **02**: 34–43.
16. Ren Ran and Liu Hongshen, 2021. An image segmentation method based on Markov random field. J. Anhui Univ. Technol. Nat. Sci. Ed. **03**: 252–255.
17. Yu Miao, Hu Zhan-Yi. Higher-order Markov random fields and their applications in scene understanding. Acta Automatica Sinica, 2015, **41** (7): 1213–1234.
18. Li Lu, Fan Wentao and Du Jixiang, 2017. Brain MR image segmentation based on Student's t mixture model with Markov random field. J. Shandong Univ. Engin. Sci. **47**: 49–55.

Qianqian Zhen and Huichao Gu. 2023. Markov random field-based segmentation algorithm for the images of cotton plants taken from unmanned aerial vehicles. Ukr.J.Phys.Opt. 24: 114 – 123.
doi: 10.3116/16091833/24/2/114/2023

Анотація. *Сегментація аерофотознімків врожаю – це важливий метод прогнозування та аналізу врожаю на основі безпілотних літальних апаратів (БПЛА) для захисту рослин. Проблема полягає в тому, що точність традиційної сегментації зображень на основі*

суперзеленого елемента недостатньо висока, а відповідний алгоритм може виявляти значні відмінності в точності для різних культур. У цьому дослідженні ми використали марковську модель випадкового поля для сегментації аерофотознімків БПЛА для захисту рослин. Для позначення поля спостереження використано стандартний алгоритм K-середнього, а параметри моделі оцінено за методом максимізації очікування. Для одкржання результатів сегментації застосовано ітерований алгоритм умовних режимів. Експериментальні результати засвідчують, що підхід випадкового марковського поля може ефективно сегментувати зображення бавовнику, отримані з БПЛА. Крім того, точність сегментації стає вищою, а алгоритм – більш адаптивним. Однак коли кількість пікселів сегментованого зображення перевищує деяке критичне значення, час опрацювання зростає, а досягнення режиму реального часу стає проблемним.

***Ключові слова**: марковське випадкове поле, ітерований алгоритм умовного режиму, безпілотні літальні апарати захисту рослин, сегментація зображення*